minerals

MDPI

Article

Location of Carbonate Ions in Metal-Doped Carbonated Hydroxylapatites

Claude H. Yoder * and Julia T. Goodman

Department of Chemistry, Franklin and Marshall College, Lancaster, PA 17604, USA; jgoodma2@fandm.edu
* Correspondence: cyoder@fandm.edu

Abstract: The environment model for the description of the location of carbonate ions in apatites predicts that approximately half of the carbonate occupies the apatite channel. This model relies on the influence of entities surrounding the carbonate on its IR spectrum and can be used to determine how various substituents affect the location and structure of that ion. Careful deconvolution (peak-fitting) of the asymmetric carbonate IR region was used to determine the percentage of A-type (channel) ions, A′-type (channel with either a Ca^{2+} vacancy or substitution of Na^{+} for Ca^{2+}) ions, and B-type (substitution for phosphate) ions. In our previous applications of this model, we have looked at the effect of alkali metal ions, such as sodium, lithium, and potassium, the ammonium ion, and the rare earth europium ion. In the present work, we explore the incorporation of the first-row transition metal ions and find that they have little effect on the location of the carbonate ion. Like the un-substituted carbonated apatite, these apatites contain about half of the carbonate in the channel, at least in derivatives that contain up to half a mole of the metal ion per mole of apatite. Attempts to incorporate greater amounts of metal ions by aqueous ion-combination reactions generally lead to lower-resolution XRD patterns and IR spectra that produce greater uncertainties in the peak-fitting modeling.

Keywords: metal-doped apatites; IR spectroscopy; environment model; carbonated apatite

Citation: Yoder, C.H.; Goodman, J.T. Location of Carbonate Ions in Metal-Doped Carbonated Hydroxylapatites. *Minerals* **2023**, *13*, 1272. https://doi.org/10.3390/min13101272

Academic Editors: Tamara Đorđević, Natalia V. Zubkova and Igor Djerdj

Received: 5 September 2023
Revised: 21 September 2023
Accepted: 26 September 2023
Published: 29 September 2023

1. Introduction

1.1. Introduction

As the principal inorganic phase in bones and teeth, carbonated hydroxylapatite has been extensively studied [1,2], most recently with a model that significantly revises the amount of carbonate in the channel [3–5]. Carbonate has long been known [1,2] to substitute for both phosphate (B-type substitution) and hydroxide (A-type substitution) in the hexagonal apatite structure (Figure 1). Metal-doped apatites have also been explored because of the possibility of adding nuances such as color, antibacterial, magnetic, or fluorescent properties to the apatite. For Cu(II), the synthetic method and temperature appear to determine the location of the copper: high-temperature solid-state techniques produce cuprate ions $(O\text{-}Cu\text{-}O)^{n-}$ (with Cu in the +1 or +2 oxidation state) in the center of the channel [6–11]. In aqueous syntheses, it appears that Cu^{2+} replaces Ca^{2+} in the Ca(2) [channel] site [12].

Studies using DFT and first-principle energy calculations [13–15] found that zinc substitution is energetically favored at the Ca(2) site relative to the Ca(1) [body] site. The formation of Zn-doped apatite was achieved above 1173K with the incorporation of linear O-Zn-O groups in the channel [16]. Products obtained by aqueous methods used the substitution of Zn^{2+} for Ca^{2+} [17].

In a natural Mn-bearing apatite, Mn^{2+}, which is smaller than Ca^{2+}, preferentially occupies the body Ca(1) site while the larger Sr^{2+} ion occupies the Ca(2) site [18]. Fe^{2+}, stabilized by the crystal field effect, substitutes in very limited amounts in the Ca(2) site [19]. Aqueous synthesis of an Fe(II) apatite (using $FeCl_2$) indicated substitution for Ca [20].

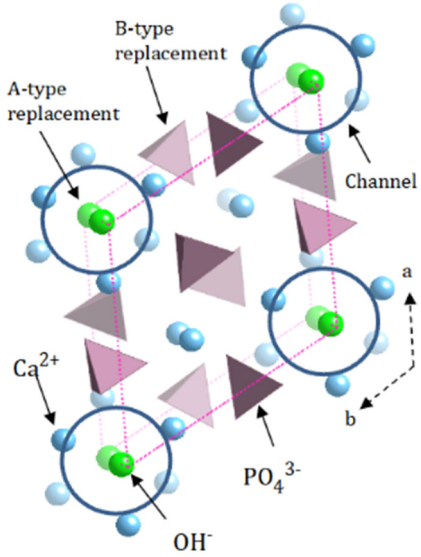

Figure 1. The structure and substitution sites in hydroxylapatite. Polyhedra designate phosphate groups (PO_4^{3-}); blue spheres represent calcium ions, with the darker spheres closer to the viewer. Green spheres are hydroxyl groups (OH^-). Circles at the corners of the unit cell indicate the positions of the channels. Calcium ions in the body of the unit cell can be designated Ca(1), while those forming the channel walls are Ca(2).

In one of the few studies of metal-doping of carbonated apatites [21], mechanical alloying of mixtures of $CaCO_3$, $CaHPO_4{\cdot}2H_2O$, and ZnO powders at room temperatures produced incorporation of Zn into the Ca(2) site with dominance of A-type carbonate, as determined by IR spectroscopy.

1.2. Objectives

The smaller size of the first-row transition metal cations relative to Ca^{2+} could lead to the stabilization of carbonate in the channel by electrostatic forces, along with the possibility of crystal field stabilization for some cations. The effect of size and crystal field stabilization can be seen in the lattice energies (kJ/mol) of the fluorides of these metals: Ca, 2611, Mn, 2770, Fe, 2912, Co, 2962, Cu, 3042, and Zn, 2971 kJ/mol. In order to test this hypothesis, we prepared and studied carbonated apatites doped with the +2 cations of Zn, Cu, Co, Fe, and Mn. The location of the carbonate ions and their surroundings has been determined using the environment model [3–5].

1.3. The Environment Model

The environment model for the assignment of the types of carbonate ions in apatites [3–5] utilizes the carbonate asymmetric stretch (ν_3) and out-of-plane bending (ν_2) regions of the IR spectrum. Deconvolution of the generally complex carbonate asymmetric stretching region (ν_3) is performed by assuming that for this region (1350 cm^{-1} to 1560 cm^{-1}), (a) there is a doublet for every structurally and environmentally distinct carbonate ion; (b) the doublet for A-type carbonate appears at a higher frequency than that of B-type carbonate; (c) the distance ($\Delta\nu$) between the members of the doublets is greater for A-type doublets; and (d) the appearance of the ν_3 region of an AB carbonated apatite can be estimated by summing the spectra of A- and B-type apatites.

It is generally acknowledged [1] that carbonate ions substituted for phosphate are designated as B-type carbonate, while those that substitute for hydroxide in the apatite channel are designated as A-type. In the environment model, A-type carbonate can be surrounded in the channel by six Ca^{2+}, or, in the case of A′-type carbonate, by five Ca^{2+} and a vacancy or by five Ca^{2+} and a sodium ion, depending on the type of charge balance that occurs during the substitution of the −2 carbonate ion for a −3 phosphate ion. In the

ν_3 region, A′-type carbonate ions generally have IR ν_3 frequencies between that of the A- and B-type ions.

Fleet [3] found evidence for three different A-type channel environments and one B-type in apatites prepared at high temperatures and pressures. For hydroxylapatites prepared in aqueous solution, carbonate ions in both A- and A′- environments have been proposed [3,4].

2. Materials and Methods

2.1. Synthesis of Carbonated Metal-Doped Apatites

Reagents were ACS reagent grade (Sigma-Aldrich, St. Louis, MO, USA) with 2.500 g $Ca(NO_3)_2 \bullet 4H_2O$, 0.898 g $(NH_4)_3PO_4$, and 0.630 g of Na_2CO_3 providing the calcium, phosphate, and carbonate for each preparation. MilliQ water was used for dissolution of reagents. The transition metal cations were used at 1:50, 1:25, and 1:10 molar ratios relative to that of calcium. The molar ratio of carbonate and phosphate was 1:1, while the molar ratio of calcium to phosphate was maintained at 1.67:1 in all preparations. ^{13}C labeled $NaHCO_3$ (99% purity) was obtained from Sigma-Aldrich. Yields were >90%. The masses of each reagent are given in Table 1.

Table 1. Masses of reactants employed in syntheses, g.

Cu	$Cu(NO_3)_2 \bullet 2.5H_2O$	$Ca(NO_3)_2 \bullet 4H_2O$	$(NH_4)_3PO_4$	Na_2CO_3
1:50	0.118	2.46	0.913	0.668
1:25	0.250	2.50	0.899	0.630
1:10	0.639	2.54	0.898	0.667
Zn	$Zn(NO_3)_2 \bullet 6H_2O$			
1:50	0.080	2.50	0.883	0.648
1.25	0.163	2,58	0.947	0.636
1.10	0.395	2.82	1.091	0.646
Co	$Co(NO_3)_2 \bullet 6H_2O$			
1:50	0.0504	2.55	0.895	0.636
1:25	0.100	2.54	0.904	0.635
1:10	0.250	2.53	0.916	0.667
Fe	$FeCl_2$			
1″50	0.0255	2.09	0.796	0.564
1:25	0.139	2.60	0.892	0.640
1:10	0.386	2.52	0.903	0.636
Mn	$Mn(NO_3)_2 \bullet 4H_2O$			
1:50	0.0745	2.55	0.898	0.545
1:25	0.139	2.60	0.892	0.640
1:10	0.386	2.52	0.903	0.636

The metal-doped carbonated apatites were prepared using two methods: the one-step method [5] and the addition method [5].

One-step synthesis. The reagents (Table 1) were added to a 125 mL Erlenmeyer flask along with 75 mL of water, and the mixture was magnetically stirred at 80 °C for one day. The pH was monitored and maintained at 8 using 3 M NH_3. The products were filtered by suction, washed four times with 50 mL of water, and dried in an oven at 110 °C for one day. The syntheses of the Fe(II)-doped compounds were run under N_2 and in the presence of elemental iron.

Addition synthesis. A 40 mL solution of $(NH_4)_3PO_4$ (Table 1) and a 40 mL solution of $Ca(NO_3)_2 \bullet H_2O$ and the metal reagent were added simultaneously at a rate of about 1 drop/s to 80 mL of the carbonate solution in a three-neck flask. The mixture was kept at 80 °C for one day with constant magnetic stirring, and the pH was maintained at 8 using 3M NH_3. The product was suction filtered, washed four times with 50 mL of water, and dried in an oven at 110 °C for one day.

2.2. Characterization

The metal-doped carbonate apatites had the following colors: Ca, white, Zn, white, Cu, blue, Co, light purple, Fe, light tan (sand), and Mn, light pink, and they were characterized using powder X-ray powder diffraction with a PANalytical X'Pert PRO Multipurpose diffractometer Theta-Theta System with Cu-K α radiation (λ = 1.54060 Å). The samples were prepared on a glass slide and analyzed using PANalytical program X'Pert Highscore Plus in a range from 6 to 70° 2θ using a step size of 0.0170 2θ and a scan step time of ca. 60 s.

IR spectra of the carbonated metal-doped apatites were obtained using a Bruker Tensor 37 IR Spectrometer with a Ge ATR mount using 256 scans and a resolution of 2 cm^{-1}. The uncertainty in peak positions obtained from multiple scans of the same sample is ±0.1 cm^{-1}. For all samples, peak-fitting was performed on spectra not modified by smoothing or baseline correction using Thermo Scientific (Waltham, MA, USA) GRAMS/AI Spectroscopy Software Suite. Peak-fitting of the carbonate asymmetric stretch region (ν_3) was based on the model that the spectral envelope is a sum of intensity due to two to four underlying doublets, the members of which are nearly equally intense [3,5]. The use of Gaussian functions for the carbonate asymmetric stretch region (ν_3) and either Gaussian or Lorentzian functions for the out-of-plane bend region (ν_2) accounted for at least 96% of the spectral intensity for most samples. The average standard error for the peak-fitting was 0.0011, as obtained from the Grams Software Suite [5]. The procedure for determining the percentages of A-, A′-, and B-type carbonate was described previously [3,5]. The determination of the uncertainty of the percentage of A in three IR spectra and deconvolutions gave an uncertainty at the 90% level of approximately 5%.

Solid-state MAS NMR spectra were obtained on an Agilent Unity 500 MHz NMR spectrometer equipped with a 3.2 mm solids probe capable of spin speeds of 24 kHz. ^{13}C spectra were obtained at 125.500 MHz using a delay time of 100 s and referenced to adamantane at 37.4 ppm. Errors in the ^{13}C chemical shifts are approximately ±0.3 ppm.

Carbonate composition was determined by combustion analysis, while metal and phosphate analyses were obtained by ICP at Galbraith laboratories (Knoxville, TN, USA). Mossbauer analysis was performed at Cornell University by Melissa Bollmeyer on a 1:25 carbonated iron-doped apatite sample prepared under N_2.

3. Results and Discussion

3.1. Composition

Compositional data and the distribution of carbonate among A, A′, and B-type [3,5] are reported in Table 2. The distribution of carbonate was determined from the IR asymmetric carbonate stretch (ν_3) region following our previous methodology [4,5].

The percentages of metal and carbonate (Table 2) indicate that, as expected, the number of moles of metal ion per gram of sample increases from the 1:50 to 1:10 samples. The molar amounts of metal ions for a given concentration level, for example, in the 1:50 samples, are reasonably uniform, except for the copper-carbonated apatites, which contain more than twice as many moles of metal ions as the other metal-doped apatites. The XRD pattern for the 1:10 copper sample indicates the presence of an amorphous constituent, perhaps tenorite (CuO). Although the presence of cuprate ions (O_2Cu^{-2}) in the channel appears to be limited to compounds prepared at high temperatures [8–13], the replacement of calcium and the formation of cuprate ions could also account for the enhanced copper content.

Table 2. Composition of selected metal-doped carbonated apatite moles per 1g of apatite.

Metal	Identification		mol M, $\times 10^{-3}$	mol CO_3, $\times 10^{-3}$	%A	%A′	%B
Cu	28	1:10	1.6	1.6	10	41	49
	32	1:25	0.83	1.1	19	39	42
	31	1:50	0.42	1.0	17	28	55
	33	1:50 *	0.56	0.94	36	19	45
Zn	35	1:25	0.41	0.97	15	41	44
	34	1:50	0.22	1.2	16	32	52
	37	1:50 *	0.23	0.79	26	32	41
Co	40	1:10	0.71	0.79	10	38	52
	39	1:25	0.29	0.92	19	28	53
	38	1:50	0.14	1.1	21	31	48
	41	1:50 *	0.1	0.69	27	27	45
Fe **	54	1:10	0.44	0.86	17	41	42
	53	1:25	0.29	0.53	15	29	56
	52	1:50	0.15	0.38	19	38	43
	55	1:50 *	0.07	0.45			
Mn	44	1:10			13	41	46
	43	1:25			13	33	54
	42	1:50	0.20	1.1	16	32	52
	45	1:50 *	0.10	0.57	38	35	27
Ca	77				16	38	46

* C-13 isotopomer prepared with $NaH^{13}CO_3$. ** Mossbauer analysis indicates that the Fe-containing apatites contain roughly equal amounts of Fe(II) and Fe(III).

The amount of metal ion present for the 1:25 series is roughly 0.3 mol metal ion per 1000 g of apatite, while the amount of carbonate for the same series is, on average, 1 mole per 1000 g. Assuming that the carbonate replaces phosphate and calcium by co-substitution of sodium (from the Na_2CO_3 used to supply carbonate) and that the metal ion replaces calcium ion, the formula should be approximately $Ca_{8.7}M_{0.3}Na(PO_4)_5(CO_3)(OH)_2$.

Analysis of the Zn 1:25 apatite for sodium (0.7%) corresponds to 0.3 mol Na^+/1000 g, and similar results for several other 1:25 and 1:50-doped apatite indicate that co-substitution of Na (with carbonate) cannot produce 1 mole of Na per mole of apatite. Thus, the co-substitution of Na is not the only charge balance mechanism operational for carbonate substitution. This is probably partly a result of the operation of the charge balance vacancy-producing mechanism:

$$CO_3^{2-} \rightarrow Ca^{2+} + PO_4^{3-} + OH^-$$

Moreover, the IR results (below) for the environment of the carbonate ion in the 1:25 apatites show that about 16% of the substitution can be attributed to the A type, which produces only the removal of hydroxide ions. Both A-type substitution and the vacancy-producing charge balance mechanism reduce the number of moles of hydroxide in the formula. Hence, our approximate formula above gives an incorrect estimate of the stoichiometry of both the sodium ion and hydroxide.

3.2. Distribution of Carbonate

The average percentages of A-, A′- and B-type carbonate, as determined by IR spectroscopy following our previously described [4,5] methodology, for the 1:25 samples are 16, 34, and 50 percent, respectively, very similar to that found (16, 38, 46 percent, respectively)

in the undoped carbonated apatite (ID = 77, Table 2). In order to determine if the carbonate location is influenced by the presence of the metal ion, the percentage of channel carbonate ions (A- + A′-type) is shown for each of the metal-doped apatites in Figure 2 and compared with the variation in lattice energies of the metal fluorides (see above). While the pattern for the metal-doped apatites is somewhat similar to the periodic pattern attributed to the crystal field effect (see Introduction), we are reluctant to make a similar attribution because of the overlapping uncertainties, which are estimated at about ±5 percent. Our conclusion is that the extent of the interaction of the carbonate ion with the metal ion is small in these compounds, and the nature of the interaction is by no means certain. Attempts to introduce greater amounts of metals into the apatite generally produced noisier IR and XRD patterns, which led to more uncertainty in the carbonate location.

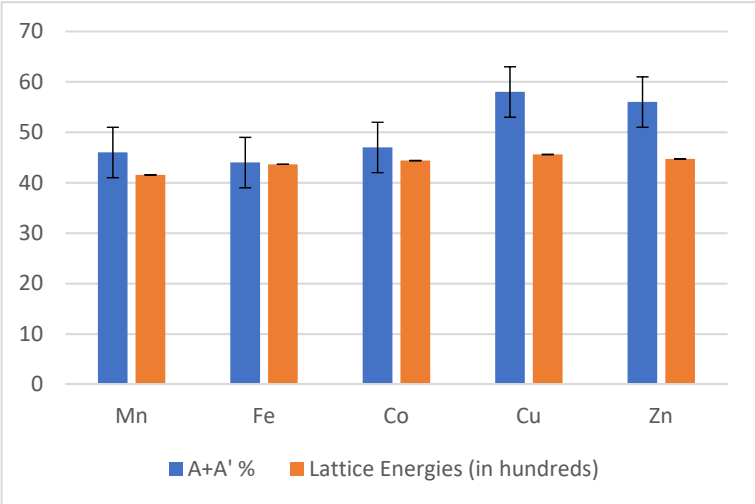

Figure 2. Comparison of percentage channel (A + A′) carbonate with lattice energies of metal fluorides. Lattice energies (see Introduction) scaled for comparison. Error bars at 5%.

3.3. ^{13}C NMR Spectroscopy and Apatites Prepared with $NaH^{13}CO_3$

The IR results can be compared to the results obtained by solid-state MAS NMR spectroscopy. The ^{13}C NMR spectrum of carbonate in the 1:50 Cu sample (ID = 33) produced a spectrum that contained two peaks: one at 164.6 ppm and a broad peak at 167.7 ppm. These peaks are shifted slightly upfield relative to the similar peaks (166.7 ppm and 170 ppm) observed for KS-117 prepared with the same reagents [5]. The upfield shift is probably a result of the paramagnetism of the copper analog, consistent with the single broad peak at 161.3 ppm for the 1:50 cobalt derivative (ID = 41). As shown previously [5], the smaller, lower frequency peak can be attributed to A-type carbonate, while the broader higher frequency peak is likely produced by overlapping peaks for A′- and B-type carbonate.

It is also instructive to compare the peak patterns for the apatites prepared with Na_2CO_3 to those prepared with $NaH^{13}C$. Table 2 shows that the percentage of A-type carbonate for the derivatives made with $NaH^{13}CO_3$ is significantly higher than for those prepared with Na_2CO_3.

For the ^{13}C labeled 1:50 apatites, these percentages range from 36 (Cu), 26 (Zn), 27 (Co), to 38 (Mn) percent. Figure 3 compares the IR carbonate ν_3 region of a 1:50 cobalt apatite prepared with $NaH^{13}CO_3$ to the same region for a 1:50 copper apatite prepared with Na_2CO_3. In addition to the presence of a high-frequency A-type peak, the other characteristic of high A-type carbonate substitution is a more intense high-frequency peak of the B-type doublet. The change in the position of the A-type peaks is presumably caused by the presence of sodium in the apatite, as has been observed previously [4]. This hypothesis was also confirmed by the observation of greater amounts of A-type carbonate in the cobalt and manganese 1:25 derivatives prepared using $(NH_4)_2CO_3$ rather than Na_2CO_3.

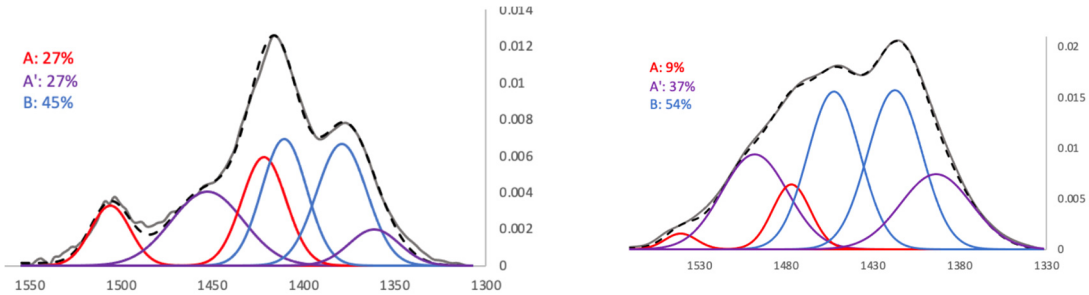

Figure 3. (**Left**), Peak-fitting following the environment model [3–5] of the (ν_3) asymmetric carbonate stretch for the ^{13}C 1:50 Co carbonated apatite prepared with $NaH^{13}CO_3$, compared with (**Right**), the ν_3 carbonate region for the 1:50 Cu carbonated apatite prepared with Na_2CO_3, which is characterized by an obvious peak at about 1510 cm^{-1} (corrected for the shift induced by the isotopic substitution; this corresponds to 1550 cm^{-1} in the C-12 isotopomer).

4. Conclusions

The amount of channel carbonate as compared to carbonate substituted for phosphate in metal-doped apatites is comparable to those amounts in undoped apatites; that is, the effect of the first-row transition metal +2 cations on the distribution of the carbonate ion in carbonated metal-doped apatites appears to be minimal. There is no evidence to support crystal field stabilization of channel carbonate by these transition metal cations. Although only 0.3 moles of metal were present in these apatites, the attempts to introduce greater amounts of metals into the apatite generally produced noisier IR spectra and XRD patterns, which led to more uncertainty in the carbonate location. In general, it appears that the variation in percent A-type carbonate is more influenced by Eu^{3+} and Na^+ substituents [22].

The use of $NaH^{13}CO_3$ rather than Na_2CO_3 in the synthesis procedure produced a greater amount of A-type carbonate, as observed previously [4].

Author Contributions: Conceptualization, C.H.Y.; methodology, J.T.G. and C.H.Y.; software, J.T.G.; validation, J.T.G. and C.H.Y.; formal analysis, C.H.Y.; investigation, C.H.Y.; resources, C.H.Y.; data curation, J.T.G.; writing—original draft preparation, C.H.Y.; writing—review and editing, C.H.Y. and J.T.G.; visualization, C.H.Y.; supervision, C.H.Y.; project administration, C.H.Y.; funding acquisition, C.H.Y. All authors have read and agreed to the published version of the manuscript.

Funding: This research was funded by the Yoder Research Fund at Franklin and Marshall College.

Data Availability Statement: Not applicable.

Acknowledgments: The authors are indebted to Emily Wilson and Beth Buckwalter of Franklin and Marshall College for technical assistance and to Melissa Bollmeyer of Cornell University for the Mossbauer analysis. The authors are also indebted to the donors of the Yoder Research Fund.

Conflicts of Interest: The authors declare no conflict of interest. The funders had no role in the design of the study; in the collection, analyses, or interpretation of data; in the writing of the manuscript; or in the decision to publish the results.

References

1. Pan, Y.; Fleet, M.E. Compositions of the apatite-group minerals: Substitution mechanisms and controlling factors. In *Reviews in Mineralogy and Geochemistry*; Kohn, M., Rakovan, J., Hughes, J.M., Eds.; Mineralogical Society of America: Washington, DC, USA, 2002; Volume 48, pp. 13–49.
2. Fleet, M.E. *Carbonated Hydroxyapatite: Materials, Synthesis, and Application*; CRC Press: Boca Raton, FL, USA, 2015.
3. Fleet, M.E. Infrared spectra of carbonate apatites: Evidence for a connection between bone mineral and body fluids. *Am. Mineral.* **2017**, *102*, 149–157. [CrossRef]
4. Yoder, C.H.; Bollmeyer, M.M.; Stepien, K.R.; Dudrick, R.N. The effect of incorporated carbonate and sodium on the IR spectra of A-, B-, and AB-type carbonate apatites. *Am. Mineral.* **2019**, *104*, 869–877. [CrossRef]
5. Yoder, C.H.; Stepien, K.R.; Dudrick, R.N. The distribution of carbonate in apatite: The environment model. *Am. Mineral.* **2023**, *108*, 1072–1079. [CrossRef]

6. Kazin, P.E.; Karpov, A.S.; Jansen, M.; Tretyakov, Y.D. Crystal structure and properties of strontium phosphate apatite with oxocuprate ions in hexagonal channels. *Z. Anorg. Allg. Chem.* **2003**, *629*, 344–352. [CrossRef]
7. Kazin, P.E.; Zykin, M.A.; Romashov, A.A.; Tret'yakov, Y.D.; Jansen, M. Synthesis and properties of colored copper-containing alkaline-earth phosphates with an apatite structure. *Russ. J. Inorg. Chem.* **2010**, *55*, 145–149. [CrossRef]
8. Karpov, A.S.; Nuss, J.; Jansen, M.; Kazin, P.E.; Tretyakov, Y.D. Synthesis, crystal structure and properties of calcium and barium hydroxyapatites containing copper ions in hexagonal channels. *Solid State Sci.* **2003**, *5*, 1277–1283. [CrossRef]
9. Pogosova, M.A.; Eliseev, A.A.; Kazin, P.E.; Azrmi, F. Synthesis, structure, luminescence, and color features of the Eu- and Cu-doped calcium apatite. *Dyes Pigment.* **2017**, *141*, 209–216. [CrossRef]
10. Pogosova, M.A.; Kalachev, I.L.; Eliseev, A.A.; Magdysyuk, O.V.; Dinnebier, R.E.; Jansen, M.; Kazin, P.E. Synthesis and characterization of the copper doped Ca-La apatites. *Dyes Pigment.* **2016**, *133*, 109–113. [CrossRef]
11. Pogosova, M.A.; Kasn, P.E.; Tretyakov, Y.D.; Jansen, M. Synthesis, structural features, and color of calcium-yttrium hydroxyapatite with copper ions in hexagonal channels. *Russ. J. Inorg. Chem.* **2013**, *58*, 381–386. [CrossRef]
12. Othmania, M.; Bachouaa, H.; Ghandoura, Y.; Alssaa, A.; Debbabi, M. Synthesis, characterization and catalytic properties of copper-substituted hydroxyapatite nanocrystals. *Mater. Res. Bull.* **2018**, *97*, 560–566. [CrossRef]
13. Terra, J.; Jiang, M.; Ellis, D.E. Characterization of electronic structure and bonding in hydroxyapatite: Zn substitution for Ca. *Philos. Mag. A.* **2002**, *82*, 2357–2377. [CrossRef]
14. Ma, X.; Ellis, D.E. Initial stages of hydration and Zn substitution/occupation on hydroxyapatite (001) surfaces. *Biomaterials* **2008**, *29*, 257–265. [CrossRef] [PubMed]
15. Matsunaga, K.; Murata, H.; Mizoguchi, T.; Nakahira, A. Mechanism of incorporation of zinc into hydroxyapatite. *Acta Biomater.* **2010**, *6*, 2289–2293. [CrossRef] [PubMed]
16. Gomes, S.; Nedelec, J.M.; Renaudin, G. On the effect of temperature on the insertion of zinc into hydroxyapatite. *Acta Biomater.* **2012**, *8*, 1180–1189. [CrossRef] [PubMed]
17. Popa, C.L.; Deniaud, A.; Michaud-Soret, I.; Guegan, R.; Motelica-Heino, M.; Predoi, D. Structural and biological assessment of zinc doped hydroxyapatite nanoparticles. *J. Nanomater.* **2016**, *2016*, 1062878. [CrossRef]
18. Hughes, J.M.; Cameron, M.; Crowley, K.D. Ordering of divalent cations in the apatite structure: Crystal structure refinements of natural Mn- and Sr-bearing apatite. *Am. Mineral.* **1991**, *76*, 1857–1862.
19. Hughes, J.; Fransolet, A.M.; Schnreyer, W. The atomic arrangement of iron-bearing apatite. *Neues Jahrb. Fur Mineral.* **1993**, *11*, 504–510.
20. Song, N.; Liiu, Y.; Zhang, Y.; Tan, Y.N.; Grover, L.M. Synthesis and characterization of iron substituted apatite. *Adv. Appl. Ceram.* **2012**, *111*, 466–471. [CrossRef]
21. Lala, S.; Ghosh, M.; Das, P.K.; Das, D.; Kard, T.; Pradhana, S.K. Structural and microstructural interpretations of Zn-doped biocompatible bone-like carbonated hydroxyapatite synthesized by mechanical alloying. *J. Appl. Crystallogr.* **2015**, *48*, 138–148. [CrossRef]
22. Stepien, K.R.; Yoder, C.H. Europium-doped carbonated apatites. *Minerals* **2022**, *12*, 503. [CrossRef]